energies

MDPI

Article

The Influence of the Shape of Granite on the Heat Storage Process in a Rock Bed

Magdalena Nemś *, Artur Nemś and Kamila Gębarowska

Department of Thermodynamics and Renewable Energy Sources, Faculty of Mechanical and Power Engineering, Wroclaw University of Science and Technology, Wybrzeże Wyspiańskiego 27, 50-370 Wroclaw, Poland; artur.nems@pwr.edu.pl (A.N.); kamila.gebarowska@pwr.edu.pl (K.G.)

* Correspondence: magdalena.nems@pwr.edu.pl; Tel.: +48-71-320-4826

Received: 13 September 2020; Accepted: 27 October 2020; Published: 29 October 2020

Abstract: Granite is one of those materials that due to its thermal parameters is used as a filling for storage beds, including high-temperature ones. The article analyzes local material that was extracted in Strzegom, Poland. The purpose of the paper is the assessment of storage material with regard to its cooperation with a heat source that is available for a short time, e.g., a solar installation. Three different shapes of granite material were tested: rock, cube and sphere. Each shape has its advantages and disadvantages, which are associated with economic and strength aspects. The article presents experimental tests of the material, which were conducted in order to determine the efficiency of the charging process. The results show that rock-shaped granite filling elements are characterized with the best parameters during the charging process, and that they obtained the highest first- and second-law efficiency in the entire tested range of inlet air temperature and flow rate. The efficiency of the cube-shaped granite was lower than the sphere-shaped granite. This means that the efficiency does not directly depend on the coefficient of sphericity of the elements that fill the storage bed. The determination of the second law efficiency showed that the highest use of energy supplied with hot air occurs after 1 h of charging the accumulator in the case of all the analyzed geometries. At the end of the paper, the influence of the obtained results on the process of modelling the charging of a storage bed filled with elements of non-spherical geometry is also discussed.

Keywords: granite bed storage; heat storage processes; thermal efficiencies

1. Introduction

Accumulation of heat is nowadays becoming more and more important due to the development of systems that use renewable energy sources, and also due to treatments that aim to improve the energy efficiency of enterprises e.g., by waste heat recovery. Among the various accumulation techniques, the use of materials such as rocks [1], preferably those that are locally available, is characterized by its simplicity, as well as many other advantages. It is worth noting that this material adapts well to a heat source and operates stably within a wide temperature range. This is an advantage when compared to accumulators that use a phase change material. It is especially important in cooperation with many renewable energy sources installations. Such a source of heat can be, e.g., a flat [2] or concentrating [3] air solar collector, which, due to the weather conditions in the climatic zone of Central Europe, works very irregularly (apart from in the summer period). The rock storage beds that are described in literature cooperate with both low-temperature [4] and high-temperature installations [5]. The chemical stability of this material and its resistance to corrosion are also important, as they affect the operational safety of rock storage beds [6].

The choice of storage bed filling material plays a significant role. In addition to the assessment of parameters such as the specific heat of the material, other parameters that affect the accumulation

process must also be evaluated. The purpose of the storage bed also plays an important role in this process [7]. The aim of this work is the assessment of three different shapes of storage material i.e., locally available Strzegom granite. The storage bed is meant to be used for permanent cooperation with a heat source with variable time availability, such as a solar concentrating collector that uses direct solar radiation. The research of other scientists often refers to the analyses and studies concerning filling materials in the form of spheres [1,8]. Yang B et al. dealt with ceramic spheres randomly poured into a cylindrical tank [9].

The maximum temperature during the tests was close to 600 °C and the material diameter was equal to 25 mm [9]. Yang J et al. in [10] analyzed the thermal performance of a storage unit with steel particles (diameters of 6 and 12 mm). In paper [11], Yang J et al. studied three shapes: spherical, flat ellipsoid and long ellipsoid. The results show that the Nusselt number was almost equal for the spheres and flat ellipsoid and was higher for the long ellipsoid. The overall heat transfer performance was the highest for the long ellipsoid. Materials with an irregular shape, such as rocks intended for solar power plants [11], as well as those with a cylindrical shape [12], and large materials such as bricks [13,14], were also investigated. The shape influences the heat storage process and the drops of pressure in a storage bed, which Allen et al. examined in [7] while investigating the impact of eight different material shapes on the drop of pressure in the system.

The efficiency of the heat accumulation process plays an important role in the assessment of the material of the storage bed. It can be determined by, e.g., the thermal efficiency of the charging process [15]. Such optimizations also use the minimization of entropy generation [16,17] and exergy efficiency [5], as well as the second-law efficiency [15,17]. The literature lacks a broader analysis of the influence of shape on the heat transfer process, and the performed analyses are carried out using various optimization methods. It is therefore difficult to compare the results of various researchers.

In the further part of the paper, the tested bed filling material is described in detail, along with the test stand and the experiment plan. Afterwards, the calculation algorithm for determining the optimization parameters is presented. The third chapter contains the results of the experimental tests and calculations. The last chapters are devoted to a discussion regarding the obtained results and the drawn conclusions from the conducted research.

2. Materials and Methods

Strzegom granite, which has high technical properties (compressive strength of 110–170 MPa [18]), high durability, and is locally available in Poland, was used in the tests. The specific heat of this material is equal to 780 J/(kg·K), which makes it attractive in terms of heat storage. It is also resistant to working in high temperatures of even several hundred degrees Celsius [19].

2.1. Filling of the Storage Bed

The three shapes of the tested filling material are shown in Figure 1. The cheapest of the considered types of material is rock granite, while the production of spheres is the most expensive. Granite cubes are characterized by the greatest stability during installation and operation, while rock and sphere granites require a special stabilizing structure. Granite cubes have the largest contact surface, followed by rock granite, with sphere granite having the smallest. This affects the heat transfer between the filling elements.

For each type of storage bed filling, a high degree of similarity regarding the arrangement of the material inside the heat accumulator was ensured. The material was selected carefully, and 230 elements with a unit weight of approximately 0.174 kg were selected for each shape. The total weight of the material in the storage bed was equal to 40.02 kg. The same mass and density allow for the assumption that the characteristic dimension, which is in the form of the substitute diameter for individual elements, was the same. The way of arranging the material inside ensured the same height of the stack, as well as the same bed filling factor of 0.65. An experiment plan was designed for the material and the tests were carried out on an experimental stand.

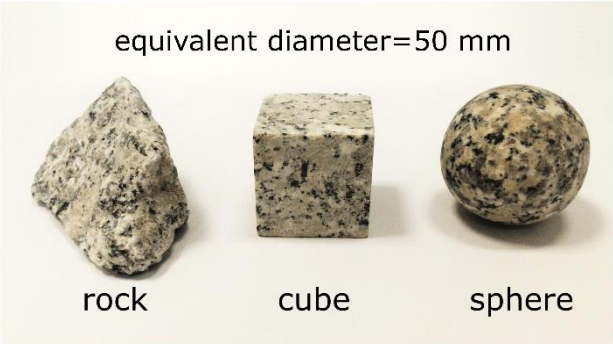

Figure 1. Photo of the tested shapes of materials that were used to fill the storage bed.

2.2. Test Stand and Experiment Plan

Figure 2 shows a diagram and photo of the stand that was used for the experimental tests of the heat storage process in the granite. The used equipment enables the air temperature at the inlet to the storage bed and the flow rate of the air sucked in from the environment to be adjusted. The measured parameters include air temperature at the inlet to the storage bed, air outlet temperature, ambient temperature, and also air flow rate.

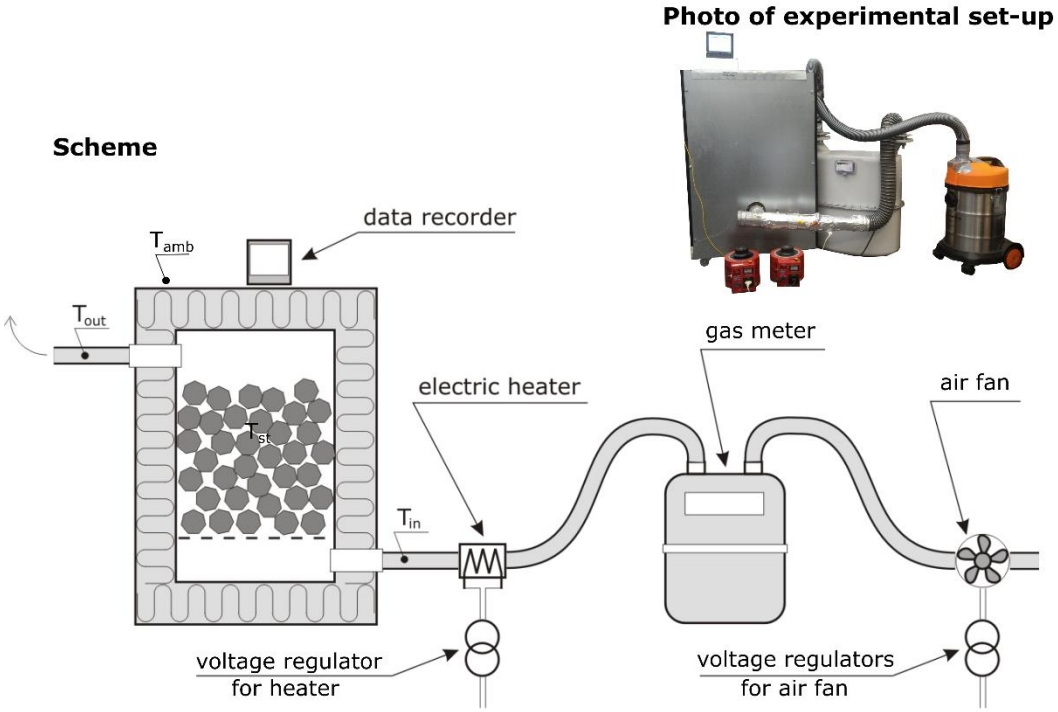

Figure 2. Schematic diagram of the stand for investigating the heat storage process.

The experimental stand is made of a metal sheet casing insulated with mineral wool. Inside, there is a chamber that can be filled with the tested material. Air is the working medium that heats the storage material. Details concerning the test stand are provided in Table 1.

Due to the multitude of results that are needed to perform a broad analysis of the operation of a storage bed with various fillings, it was decided to use an experiment plan with a shortened testing time. The input factors, which are important for the heat storage process, include the air temperature at the inlet to the bed T_{air_inlet}, and its volumetric flow rate $\dot{V}_{air}$. The design of the Hartley experiment, which was described in detail in [19,20], was selected for the investigation. It enabled the tests to be carried out for three input factors at three levels of variation. The sphericity of the examined granite

elements, which was marked as Ψ and determined on the basis of [21], was defined as the third factor. Parameter Ψ for the rock granite was equal to 0.6, for the cube granite to 0.8, and for the sphere granite to 1.0. Table 2 summarizes the input factors with three levels of variability, which were determined according to the principles described in [20].

Table 1. Parameters of the experimental set-up.

Rock Bed	Internal Height	b	0.5 m
	Internal thickness	a	0.3 m
	Internal length	a	0.3 m
Storage Material	Specific heat	c_{p_mat}	780 J/(kg·K)
	Mass	m_{mat}	0.174 kg
	Number of elements	n	230
Insulation	Top insulation thickness	δ_{ins_top}	0.20 m
	Bottom insulation thickness	δ_{ins_bot}	0.15 m
	Side insulation thickness	δ_{ins_side}	0.15 m
	Thermal conductivity	λ_{ins}	0.039 W/(m·K)

Table 2. Assumed values of input factors.

Variable	**−1**	**0**	**+1**
Ψ, -	0.6	0.8	1.0
T_{air_inlet}, °C	80	110	140
$\dot{V}_{air}$, m^3/s	0.006	0.008	0.010

Table 3 shows the matrix of the Hartley design for the performed experiment. In accordance with these settings, the test stand arrangements and bed filling material were prepared for each of the 11 experiments, and then the tests were carried out. The use of the experimental plan during the tests enables the final equation for the selected parameter (characterizing the heat accumulation process) to be determined. This facilitates the analysis of the selected shape of the material in the given temperature and flow ranges.

Table 3. Hartley design matrix for the experimental tests.

No.	Ψ	T_{air_in}	$\dot{V}_{air}$
	-	°C	m^3/s
1	1.0	140	0.010
2	1.0	80	0.006
3	0.6	140	0.006
4	0.6	80	0.010
5	1.0	110	0.008
6	0.6	110	0.008
7	0.8	140	0.008
8	0.8	80	0.008
9	0.8	110	0.010
10	0.8	110	0.006
11	0.8	110	0.008

During the experimental tests for the given autotransformer settings, the volumetric flow rate and the level of the inlet temperature to the bed were monitored. Data from thermocouples were recorded at one-minute increments.

In order to carry out comparative analyses for the indicated three shapes of granite, it was required to first calculate the average temperature of the material inside the bed. For this purpose, it was necessary to perform the thermal balance of the accumulator, which is described in the next section.

2.3. Thermal Balance of the Storage Bed

The temperature of the storage bed's filling material is used in the calculations of entropy generation. This temperature cannot be measured due to the temperature gradient within the bed, which is a result of the heat exchanged along the accumulator from the inlet to the outlet, and the fact that air flows unevenly through the bed. Therefore, for further calculations, it was necessary to determine the average temperature of the accumulator's filling material. Knowing the parameters of the air at the inlet and outlet of the bed, and the material parameters of the casing, it was possible to make a thermal balance of the amount of heat supplied with hot air $\dot{Q}_{input}$ and the heat losses from the surface of the accumulator $\dot{Q}_{loss\_all}$. This allowed the amount of stored energy $\dot{Q}_{accu}$ (1) and the average temperature of the storage bed's filling material T_{mat} to be determined from (2).

$$\dot{Q}_{accu} = \dot{Q}_{input} - \dot{Q}_{loss\_all} \tag{1}$$

$$\dot{Q}_{accu} = \frac{n \cdot m_{mat} \cdot c_{p\_mat} \cdot (T_{mat\_i+1} - T_{mat\_i})}{\Delta t} \tag{2}$$

The flux of the supplied heat $\dot{Q}_{input}$ is described by Equation (3).

$$\dot{Q}_{input} = \dot{m}_{air} \cdot c_{p\_air} \cdot (T_{air\_inlet} - T_{air\_outlet}) \tag{3}$$

where the specific heat of air at a constant pressure c_{p_air} is calculated as in the case of a semi-perfect gas for which the temperature is the average value T_{air_avg} of the inlet and outlet air temperatures. The mass flow rate $\dot{m}_{air}$ is derived from (4) while assuming that the air is treated as a semi-perfect gas, where density ρ_{air} is a function of the inlet temperature T_{air_inlet}. This is because the volumetric flow rate $\dot{V}_{air}$ is measured at the air inlet of the accumulator.

$$\dot{m}_{air} = \dot{V}_{air} \cdot \rho_{air} \tag{4}$$

Heat losses from the surface of the accumulator $\dot{Q}_{loss\_all}$ (5) take into account the losses from the four sidewalls $\dot{Q}_{loss\_side}$, and also the top $\dot{Q}_{loss\_top}$ and bottom $\dot{Q}_{loss\_bot}$ surfaces.

$$\dot{Q}_{loss\_all} = 4\dot{Q}_{loss\_side} + \dot{Q}_{loss\_top} + \dot{Q}_{loss\_bot} \tag{5}$$

The tests were carried out in a laboratory, and therefore it is assumed that there was convective heat exchange between the walls and the environment outside the accumulator. The occurrence of radiation heat exchange was also taken into account. The accumulator was placed on wheels that are used for transport, and thus there was also a free convection on the bottom surface. Due to the fact that the level of filling in the accumulator was equal to 0.65, the speed of the air flowing through the accumulator was small. As a result, the performed heat loss calculations for the forced convection inside the accumulator gave a lower value than for the free convection. Due to the fact that a higher value is always considered in loss calculations, only the algorithm for determining heat losses is presented below. The algorithm also uses the equations for free convection on the inner side of each wall of the storage bed.

In the heat loss calculations that take into account the occurrence of free convection on both sides of the accumulator's casing, there are unknowns T_{in}, Gr_{in}, Nu_{in}, h_{c_in}, T_{out}, Gr_{out}, Nu_{out}, h_{c_out}, h_{r_out}, and $\dot{Q}_{loss}$. They are determined for each surface of the accumulator. This means that there is a need to determine 30 unknowns that describe the process of the heat losses from the accumulator. For this purpose, a set of equations was created for the process of heat transfer to the environment through all the surfaces of the accumulator.

The Grashof number is determined from Equation (6).

$$Gr = \frac{g \cdot x^3 \cdot \beta \cdot \Delta T}{\nu^2} \tag{6}$$

In the heat exchange inside the accumulator, the characteristic dimension is: for the side of the bed, it is its height b; and for the top and bottom surfaces, it is c_h [22], which is given by (7).

$$c_h = \frac{1}{\frac{1}{a} + \frac{1}{a}} \tag{7}$$

where a is the width and length of the bed. The temperature difference ΔT inside the accumulator: for the side surface is $T_{air\_avg} - T_{in\_side}$, for the top surface is $T_{air\_avg} - T_{in\_top}$, and for the bottom surface is $T_{air\_avg} - T_{in\_bot}$. The linear coefficient of expansion β is calculated for the average value of the temperature of the layer adjacent to the wall for each of the surfaces of the accumulator. It is similar to the kinematic viscosity ν, which is a function of the average temperature of the layer adjacent to the wall for the assessed surface.

The Nusselt number Nu_{in} is determined from Equation (8) [22].

$$Nu_{in} = 0.75 \cdot \left(Gr_{in} \cdot Pr_{avg}\right)^{\frac{1}{4}} \cdot \left(\frac{Pr_{avg}}{Pr_{wall}}\right)^{\frac{1}{4}}, \tag{8}$$

where the Prandtl number Pr_{avg} is determined for the average fluid temperature T_{air_avg}, and Pr_{wall} is determined for the wall temperature T_{in}.

The convective heat transfer coefficient is described by Equation (9). For the top surface, it is increased by 30%, and for the bottom surface, it is decreased by 30%.

$$h_c = \frac{\lambda_{air} \cdot Nu}{x} \tag{9}$$

For the outer side surface of the accumulator, the characteristic dimension is the height that is equal to $b + \delta_{ins\_top} + \delta_{ins\_bot}$, while for the top and bottom surfaces it is d_h, which is expressed by (10).

$$d_h = \frac{1}{\frac{1}{a+2\delta_{ins\_side}} + \frac{1}{a+2\delta_{ins\_side}}} \tag{10}$$

The Nusselt number Nu_{out} for the external surfaces is described by general Equation (11):

$$Nu_{out} = C \cdot \left(Gr_{out} \cdot Pr_{out}\right)^k, \tag{11}$$

where the constants are as follows:

$C = 0.5$, $k = 0$ if $Gr \cdot Pr < 10^{-3}$.
$C = 1.18$, $k = 1/8$ if $10^{-3} < Gr \cdot Pr < 500$.
$C = 0.54$, $k = 1/4$ if $500 \leq Gr \cdot Pr < 2 \cdot 10^7$.
$C = 0.135$, $k = 1/3$ if $2 \cdot 10^7 \leq Gr \cdot Pr$.

The Grashof and Prandtl numbers are determined analogously to those determined for the inside of the accumulator. Only the characteristic dimensions and the selected temperature differences are changed. The Prandtl number and the physical properties that occur in the Grashof number are determined for the average temperature of the layer adjacent to the wall. Moreover, radiative heat exchange occurs outside the accumulator and is described by the radiative heat transfer coefficient h_{r_out}, which is determined from Equation (12).

$$h_{r\_out} = \frac{\varepsilon_{wall} \cdot \sigma \cdot \left(T_{out}^4 - T_{amb}^4\right)}{T_{out} - T_{amb}} \tag{12}$$

From Equation (6), the Grashof number for the heat transfer inside and outside the accumulator was determined. The Nusselt numbers were determined from Equations (8) and (11), and the convective heat transfer coefficient for both sides of the partition were determined from Equation (9). The radiative coefficient of heat transfer to the outside of the accumulator was calculated from Equation (12). Therefore, seven equations describing the process of heat transfer through the partition are obtained. The last three equations for determining all ten unknowns for each of the surfaces are general equations for the heat transfer through the surface of the accumulator $\dot{Q}_{loss}$. The first Equation (13) describes the heat transfer on the inside of the accumulator.

$$\dot{Q}_{loss} = A_{in} \cdot \left(T_{air\_avg} - T_{in} \right) \cdot h_{c\_in} \tag{13}$$

The heat flux that enters the partition is equal to the heat flux received on the other side, which for the analyzed accumulator is described by Equation (13).

$$\dot{Q}_{loss} = A_{out} \cdot (T_{out} - T_{amb}) \cdot (h_{c\_out} + h_{r\_out}) \tag{14}$$

The third equation takes into account the heat flux conducted through the wall. It is equal to the heat flux determined from Equations (13) and (14) and is expressed by formula (15).

$$\dot{Q}_{loss} = A_{part} \cdot (T_{in} - T_{out}) \cdot \frac{\delta_{ins}}{\lambda_{ins}} \tag{15}$$

In Equation (15), the surface area is the average value of the partition's surface area. Due to the fact that it varies linearly from A_{in} inside the accumulator to A_{out} outside the accumulator, it can be written as (16):

$$A_{part} = \frac{A_{in} + A_{out}}{2} \tag{16}$$

The ten equations described above allowed for the determination of ten unknowns that describe the heat exchange process between the air flowing inside the accumulator and the environment for one surface. The total heat losses from the bed $\dot{Q}_{loss\_all}$, which are described by Equation (5), take into account three surfaces. Therefore, these equations were written for each of the surfaces, resulting in a system of 30 equations. In order to determine the searched average bed temperature, Equations (1)–(3) were added to the thermal balance, and the system of 33 equations and 33 numerically determined unknowns was created. The average granite temperature, determined in this way, was used in the optimization analysis, which is discussed in the next part of the paper.

2.4. Calculation of the First-Law and Second-Law Efficiencies

The collected experimental data and the results of the heat balance allowed the thermal efficiency of the process and the entropy generation to be specified in order to determine the second-law efficiency.

There are many definitions of the first law of thermodynamics, also known as the first-law efficiency [23]. However, they mean the same and result from the energy balance. Generally, the first-law efficiency can be defined as the quotient of the energy effect obtained for the system in question, and the energy supplied to this system. It is written as (17).

$$\eta_1 = \frac{Energy\ effect}{Energy\ supplied} \tag{17}$$

The first-law efficiency for heat accumulators was written, e.g., by Bejan [17] as (18).

$$\eta_1 = \frac{Q_{stored}}{Q_{\max\_stored}} \tag{18}$$

For the analyzed case, it can be written as (19):

$$\eta_1 = \frac{n \cdot m_{mat} \cdot c_{p\_mat} \cdot \left(T_{mat\_final} - T_{mat\_start}\right)}{n \cdot m_{mat} \cdot c_{p\_mat} \cdot \left(T_{air_{in}} - T_{mat\_start}\right)} \tag{19}$$

Then, the thermal efficiency of the heat accumulator's charging process, also called the first-law efficiency, was derived in [15] and presented as (20).

$$\eta_1 = 1 - e^{-y\theta} \tag{20}$$

The introduced dimensionless time θ is expressed by (21).

$$\theta = \frac{\dot{m}_{air} \cdot c_{p\_air}}{n \cdot m_{mat} \cdot c_{p\_mat}} \cdot t \tag{21}$$

The heat exchanger's parameter y is expressed as (22).

$$y = 1 - e^{-N_{tu}} \tag{22}$$

The number of heat transfer units N_{tu} is determined from dependencies (23) [17].

$$e^{-N_{tu}} = \frac{T_{air\_outlet} - T_{mat}}{T_{air\_inlet} - T_{mat}} \tag{23}$$

Calculations related to the concept of entropy and exergy were carried out. Cengel and Boles [23] define the second-law efficiency as a measure of approximation to a reversible process. Therefore, such efficiency for any system can be written as (24).

$$\eta_2 = \frac{Exergy\ recovered}{Exergy\ supplied} \tag{24}$$

According to the investigation conducted by Bejan [17], it can be expressed by (25). For the case of the storage processes, Equation (26) was used to estimate the value of the entropy generation rate $\dot{S}_{gen}$ [17].

$$\eta_2 = \frac{T_{amb} \cdot \dot{S}_{gen}}{E_x} \tag{25}$$

$$\dot{S}_{gen} = \dot{m}_{air} \cdot c_{p\_air} \cdot ln\left(\frac{T_{amb}}{T_{air\_inlet}}\right) + \frac{\dot{Q}_{out}}{T_{amb}} + n \cdot m_{mat} \cdot c_{mat} \cdot \frac{dT_{mat}}{dt} \tag{26}$$

where $\dot{Q}_{0ut}$ is the heat transfer to the environment, which was calculated from (27).

$$\dot{Q}_{0ut} = \dot{m}_{air} \cdot c_{p\_air} \cdot (T_{air\_outlet} - T_{amb}) \tag{27}$$

The dimensionless temperature τ is expressed by (28).

$$\tau = \frac{T_{air\_inlet} - T_{amb}}{T_{amb}} \tag{28}$$

Moreover, the total supplied exergy was estimated using Equation (29) on the basis of [17].

$$E_x = \dot{m}_{air} \cdot c_{p\_air} \cdot t \cdot \left(T_{air\_inlet} - T_{amb} - T_{amb} \cdot ln\left(\frac{T_{air\_inlet}}{T_{amb}}\right)\right) \tag{29}$$

The results of measurements and calculations are presented graphically in the next chapter.

3. Results

The analysis of the influence of the shape of granite on the charging process of the heat accumulator was based on the well-known thermal efficiency of the process. The change in efficiency over time was shown for different temperatures of air entering the accumulator and for different flow rates in order to determine the influence of these parameters on the analyzed geometries of the granite. Thermal efficiency does not define the charging time of an accumulator, and therefore it is worth checking the second-law efficiency, which provides information regarding this matter.

3.1. Experimental Research Results

The ambient temperature was around 22 °C during all the experiments. Figure 3 shows the results of the measurements of the air flowing out of the bed, with the measuring points being designated every 10 min for better orientation. The various inlet temperatures are marked with colors, while the shape of the filling material and the volumetric air flow rate are marked with symbols.

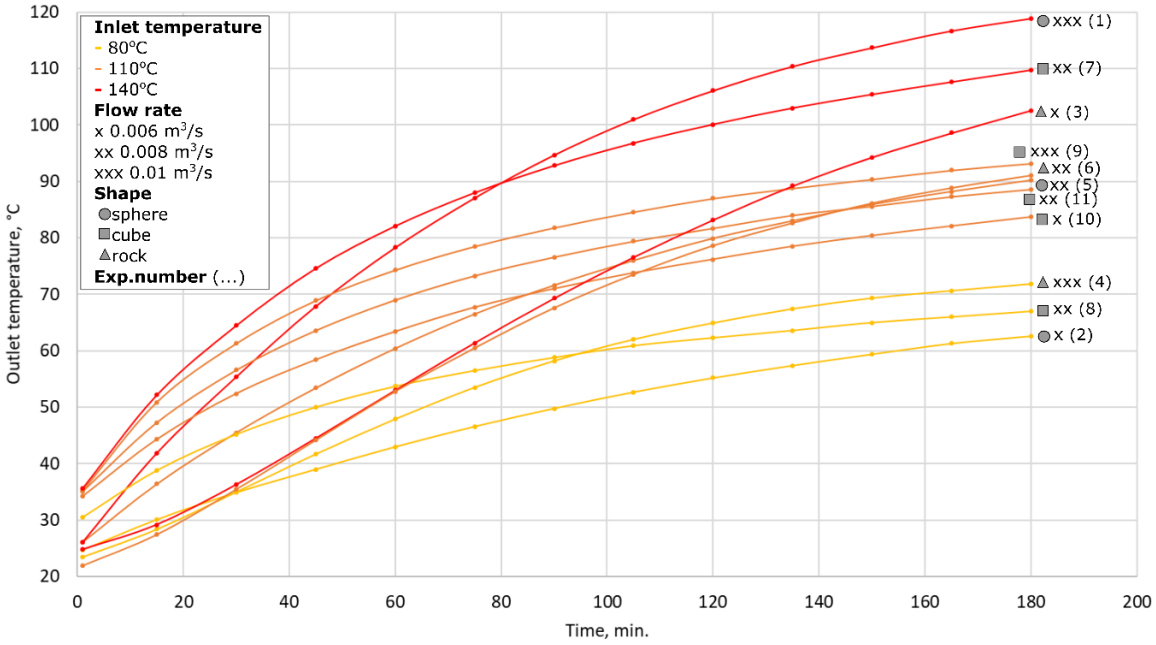

Figure 3. Changes in air outlet temperature during the charging process of the bed.

The temperature characteristics shown in the graph tend to flatten. Such flattening took place almost completely in the subsequent hours of the charging process. Due to the purpose of the comparative research carried out in the article, only the first three hours of the process were analyzed, which are very important with regard to the cooperation between the rock bed and the heat source, which is available for a short time. In the first minutes of charging, the curves for rock granite are almost linear in all the tested cases. The lowest achieved outlet temperature may be due to the intense heat transfer at this time. The less streamlined shape of the rock-shaped granite can cause a more turbulent flow, while at the same time increase the heat transfer.

During the tests, drops in pressure in the bed were also measured, and in the tested range they were not dependent on the shape of the material, but instead only on the volumetric flow rate. For the lowest flow of 0.006 m^3/s, the pressure drop in the bed was equal to 3 Pa; for 0.008 m^3/s, the pressure drop in the bed was equal to 5 Pa; and for 0.010 m^3/s, the pressure drop was equal to 7 Pa. This means that the amount of energy lost to overcome hydraulic resistances is many times smaller than the transferred thermal energy. Therefore, further analyses omit the influence of hydraulic drops on the second-law efficiency.

3.2. Thermal Efficiency of the Charging Process

The used Hartley design serves as a means to generate a quadratic equation describing the unknown parameter y_{exp} with the use of three independent variables. In the analyzed case, a series of eleven experiments, performed in accordance with the design, allow the following polynomial to be obtained (30).

$$y_{exp} = b_o + b_1 \cdot T_{air\_inlet} + b_2 \cdot T^2_{air\_inlet} + b_3 \cdot \Psi + b_4 \cdot \Psi^2 + b_5 \cdot \dot{V}_{air} + b_6 \cdot \dot{V}^2_{air} + b_7 \cdot T_{air\_inlet} \cdot \Psi + b_8 \cdot T_{air\_inlet} \cdot \dot{V}_a + b_9 \cdot \Psi \cdot \dot{V}_{air} + b_{10} \cdot T_{air\_inlet} \cdot \Psi \cdot \dot{V}_{air} \quad (30)$$

where $b_0, b_1, \ldots, b_{10}$ are regression coefficients. Due to the use of the experiment plan, the equations were determined. Thanks to this, the spatial characteristics of the change in the given parameters within the range of the assumed boundary conditions, which are defined in Table 2, were plotted. In the first step, Equation (30) was used to determine the first-law efficiency, which resulted in the creation of the 3D graphs as shown in Figure 4. The characteristics shown in Figure 4 present the change in thermal efficiency over time within the examined temperature range and mass flow rate.

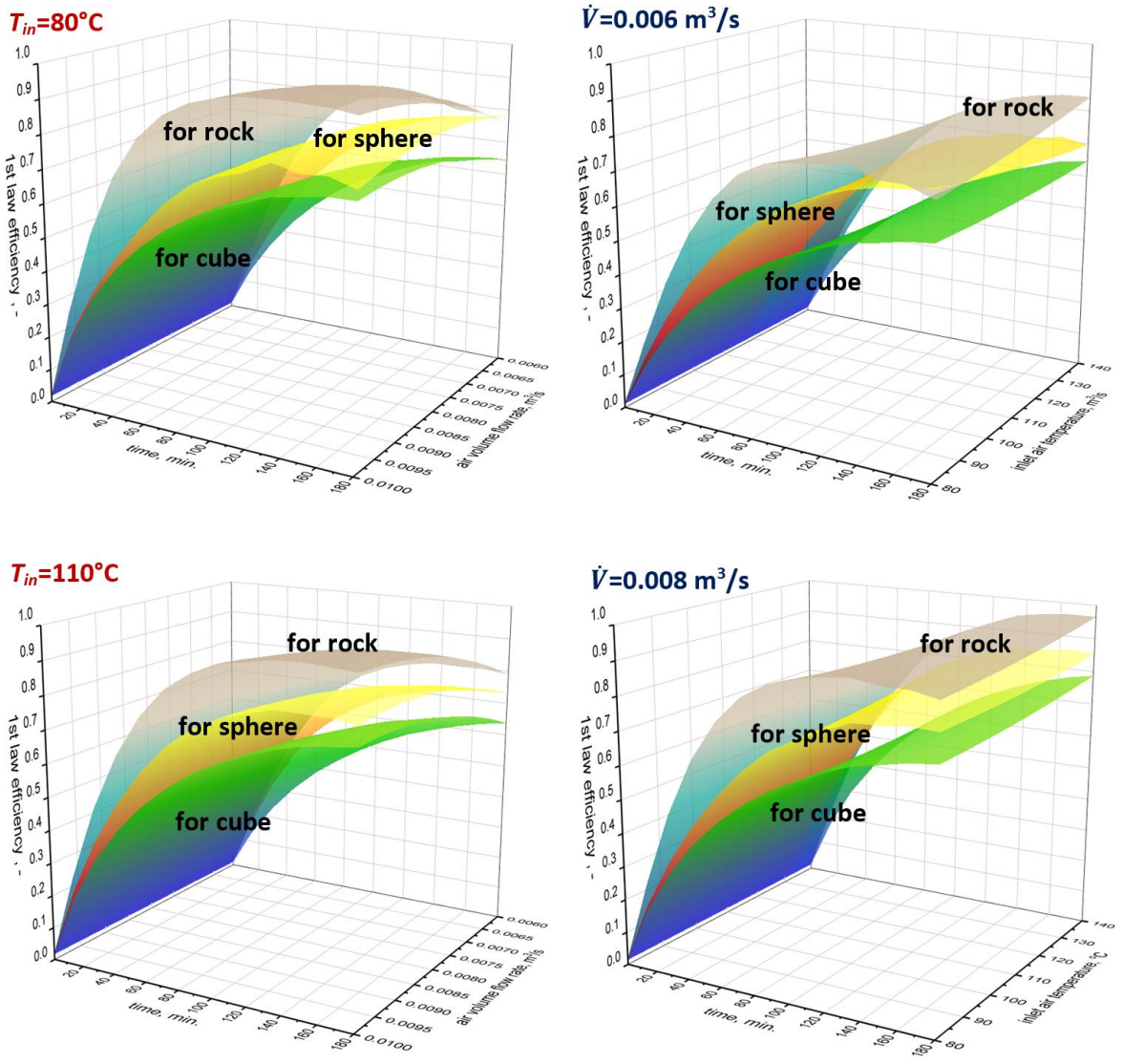

Figure 4. *Cont.*

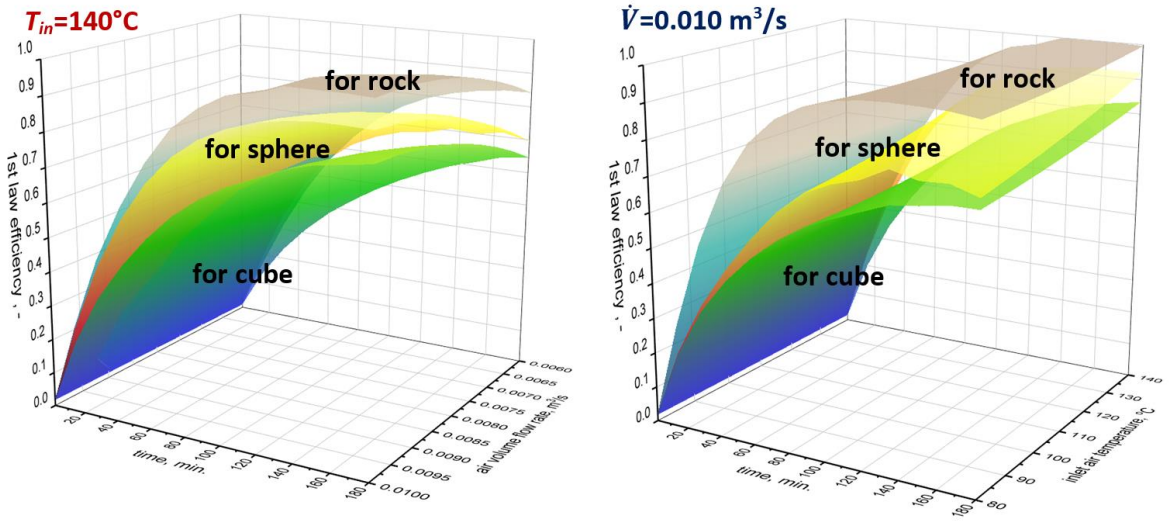

Figure 4. Changes in the first-law efficiency over time for the tested temperature range and flow rate.

As can be seen from Figure 4, the highest thermal efficiency in all the analyzed cases is achieved for rock granite. Lower values are obtained for sphere granite, and the lowest values for cube granite. The biggest differences are between the 60th and the 100th minute of charging and are especially visible for the highest flow and lowest inlet temperature. However, the influence of temperature and flow rate on the thermal efficiency for each of the analyzed geometries is not large. The charging time, i.e., the changing temperature of the air and granite, has a much greater influence. Therefore, it is worth analyzing the accumulator's charging process with regard to the second-law efficiency.

3.3. The Generation of Entropy—The Second-Law Efficiency

By performing calculations of the generation of entropy, the total exergy content of the air drawn from the hot air supply, and by applying the experiment plan, it was possible to plot the change in the second-law efficiency over time for the examined area of the air inlet temperature and the flow rate (Figure 5). The calculations were also conducted with the use of the method described in Section 3.2 and Equation (30), but this time in order to determine the second-law efficiency.

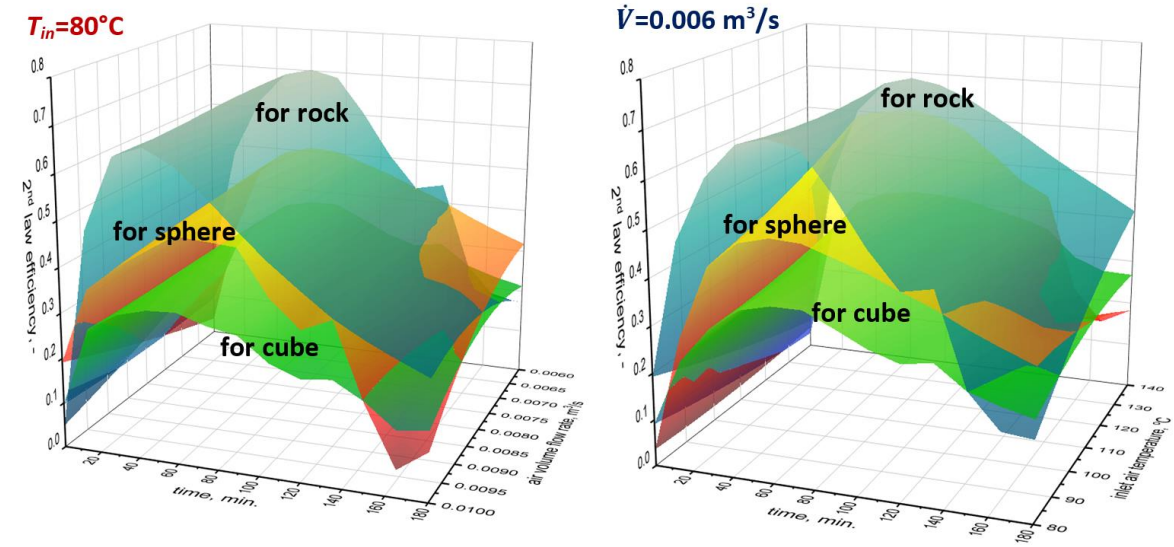

Figure 5. *Cont.*

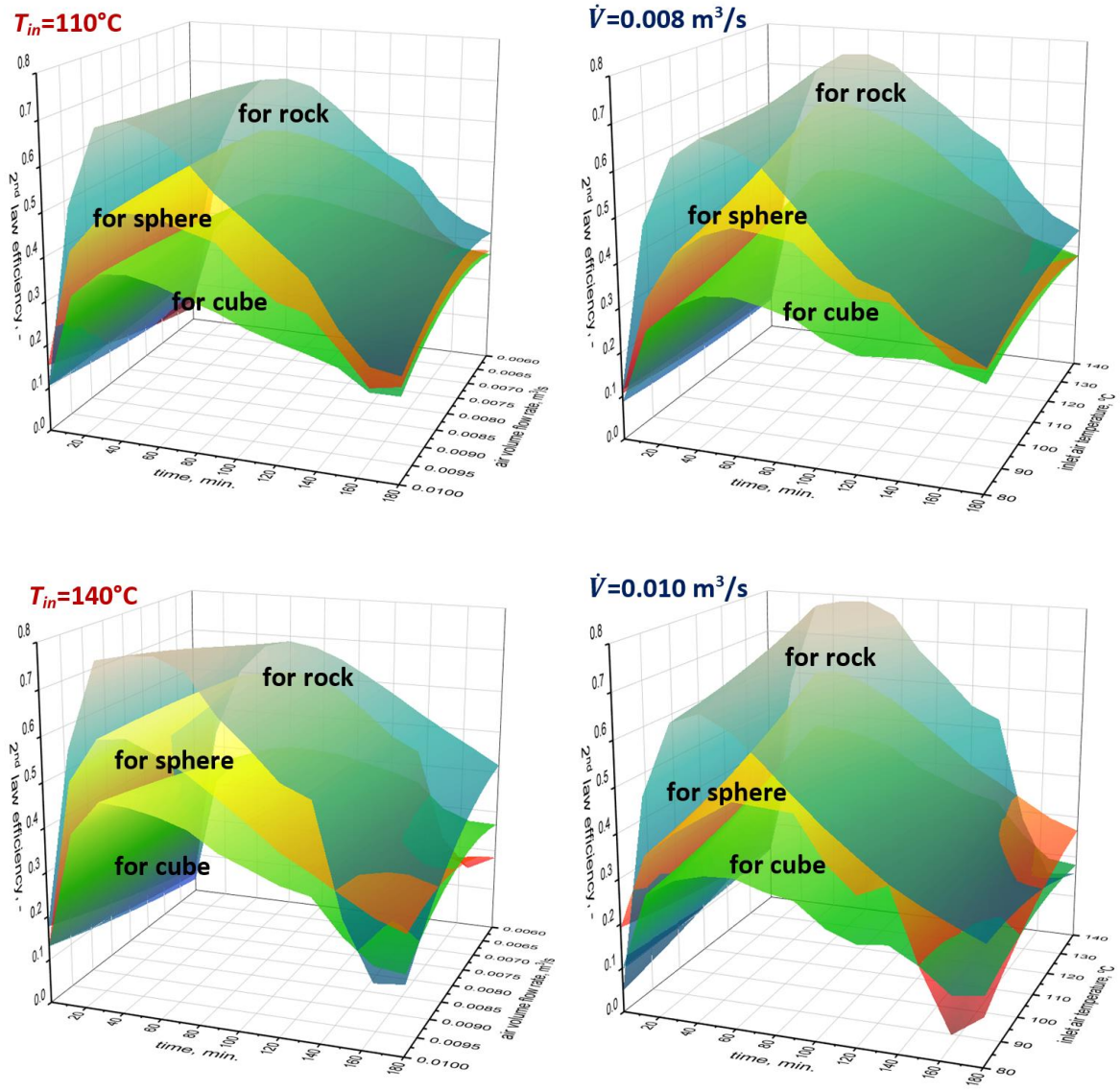

Figure 5. Changes in the second-law efficiency over time for the tested temperature range and flow rate.

The determined second-law efficiency achieves the highest values for rock granite in almost the entire tested range, and the lowest values for cube granite. As can be seen from Figure 5, the efficiency of the charging process for rock granite reaches the highest values after 60 min for the highest inlet air temperature. For the sphere and cube granites, the second-law efficiency also reaches the highest values after 1 h. However, after this time, the efficiency for rock granite drops very quickly, and reaches the lowest values at the end of the measurements for the entire tested range of the flow rate. For the charging time shorter than 2 h, the use of the energy potential for the cube and sphere granites is smaller than for the rock granite. For these geometries, the second-law efficiency decreases slower over time.

4. Discussion and Conclusions

The literature review showed a negligible amount of papers concerning the influence of the geometry of heat accumulator filling elements on the efficiency of the storage process. This especially applies to materials with a non-spherical geometry. Therefore, the authors prepared appropriate research materials and performed experiments based on the experimental plan. The results of different outlet air temperatures were obtained for different granite geometries and the same initial conditions. It

was shown that the geometry of the accumulator's filling elements affects the thermal efficiency of the charging process. In the entire tested range, the highest efficiency was obtained for rock granite, which is characterized by the lowest coefficient of sphericity. The process of charging an accumulator filled with sphere granite has a lower efficiency, and the lowest efficiency is obtained for an accumulator filled with cube granite. This means that the coefficient of sphericity is not a parameter that determines the charging efficiency.

The determination of the second-law efficiency enabled the degree of using the energy supplied with hot air to be determined. The change in this efficiency over time showed that the best use of the supplied energy is obtained after 1 h. The efficiency then reaches the highest values for all the tested geometries. However, the charging process is most intensive for rock granite and the least intensive for cube granite. As a result, rock granite, apart from its attractive price, also has the best geometry with regard to thermal analysis due to its non-spherical surface.

Finally, it is worth noting that during the model calculations, the flux of the heat transferred between hot air and the material filling the accumulator $\dot{Q}_{accu}$ can be determined from Equation (31). This means that this flux for the same starting temperatures of air and granite depends only on the heat transfer coefficient h and the heat transfer surface area A_{mat}.

$$\dot{Q}_{accu} = n \cdot h \cdot A_{mat} \cdot \left(T_{air\_avg} - T_{mat} \right) \tag{31}$$

Literature provides formulas for the Nusselt number for the determination of the heat transfer coefficient, which were developed by Ranz and Marchall [24], Kacnelson and Timofiejewa [25], Ketterning [26], and Delton [27]. The characteristic dimension is the diameter of the material, or the equivalent diameter, which is calculated from the volume of the sphere. This means that when modelling an accumulator filled with elements with the investigated geometry, the heat transfer flux $\dot{Q}_{accu}$ should assume the same values. However, as the research shows, the differences between the various geometries are visible. This is mainly due to the different heat exchange surface, the contact surface between the elements of the accumulator's filling, or the different flow around non-spherical bodies. Therefore, according to the authors, the modelling of the heat storage in materials with complex geometry requires deeper analysis and should be subjected to further research.

Author Contributions: Conceptualization, M.N.; methodology, M.N. and A.N.; validation, M.N. and A.N.; investigation, K.G.; writing—original draft preparation, M.N.; writing—review and editing, M.N. and A.N.; visualization, M.N.; formal analysis, A.N.; funding acquisition, M.N. All authors have read and agreed to the published version of the manuscript.

Funding: This research was funded by the Ministry of Science and Higher Education in Poland within the grant for Wrocław University of Science and Technology. Project no. 0402/0171/18 and 8201003902.

Conflicts of Interest: The authors declare no conflict of interest.

Nomenclature

a	internal width and length of the bed, m
A_{in}	the area of the inner wall of the bed, m^2
A_{mat}	area of single element of granite in storage bed, m^2
A_{out}	the area of the outer wall of the bed, m^2
A_{part}	the average value of the partition's surface area, m^2
b	internal height of the bed, m
$b_0, b_1, \ldots, b_{10}$	regression coefficients from Hartley plan of experiment
C	constant
c_h	characteristic dimension of the upper and lower inner surface of the bed, m
c_{p_air}	specific heat of air at constant pressure, J/(kg·K)
c_{p_mat}	specific heat of the granite storage material, J/(kg·K)
d_h	characteristic dimension of the upper and lower outer surface of the bed, m
E_x	flow exergy, J

Gr	Grashof number
h	convection heat transfer coefficient, W/(m^2·K)
h_{c_in}	convective heat transfer coefficient on the inside of the bed, W/(m^2·K)
h_{r_out}	radiative heat transfer coefficient on the outer side of the bed, W/(m^2·K)
k	constant
$\dot{m}_{air}$	mass air flow rate, kg/s
m_{mat}	mass of single element of granite in storage bed, kg
n	amount of granite elements in storage bed
N_{tu}	number of heat transfer units
Nu	Nusselt number
Pr_{avg}	Prandtl number calculated for the average temperature of the working medium
Pr_{wall}	Prandtl number calculated for the mean wall temperature
$\dot{Q}_{accu}$	stream of accumulated heat, W
$\dot{Q}_{input}$	heat flux supplied with hot air, W
$\dot{Q}_{loss}$	heat loss flux from the surface of the bed, W
$\dot{Q}_{loss\_all}$	total heat loss flux from the bed surfaces, W
$\dot{Q}_{out}$	heat transfer to the ambient, W
$\dot{S}_{gen}$	entropy generation rate, W/K
t	time, s
T_{amb}	ambient temperature, °C
T_{air_avg}	average air temperature inside the bed, °C
T_{air_inlet}	inlet air temperature, °C
T_{air_outlet}	outlet air temperature, °C
T_{in}	temperature of the inner wall surface of the bed, °C
T_{mat}	granite temperature, °C
T_{out}	temperature of the outer wall of the bed, °C
$\dot{V}_{air}$	volumetric air flow rate, m^3/s
x	characteristic dimension, m
y	heat exchanger parameter
y_{exp}	unknown parameter from Hartley plan of experiment, (variable)
Greek symbols	
v	kinematic viscosity, m^2/s
β	thermal expansion coefficient, 1/K
η_1	first-law efficiency
η_2	second-law efficiency
θ	dimensionless time
ρ_{air}	density of the air, kg/m^3
τ	dimensionless temperature
δ_{ins}	insulation thickness, m
λ_{air}	thermal conductivity of air, W/(m·K)
λ_{ins}	thermal conductivity of the insulation, W/(m·K)
ε_{wall}	the emissivity coefficient of the outer wall of the storage bed
Ψ	the sphericity
Δt	time step, s
Index	
bot	bottom surface of the bed
in	inside the bed
out	outside the bed
side	side surface of the bed
top	top surface of the bed

References

1. Gautam, A.; Saini, R.P. A review on technical, applications and economic aspect of packed bed solar thermal energy storage system. *J. Energy Storage* **2020**, *27*, 101046. [CrossRef]
2. Singh, S. Thermohydraulic performance of double pass solar thermal collector with inline, staggered and hybrid fin configurations. *J. Energy Storage* **2020**, *27*, 101080. [CrossRef]
3. Bellos, E.; Tzivanidis, C.; Daniil, I.; Antonopoulos, K.A. The impact of internal longitudinal fins in parabolic trough collectors operating with gases. *Energy Convers. Manag.* **2017**, *135*, 35–54. [CrossRef]
4. Singh, H.; Saini, R.P.; Saini, J.S. A review on packed bed solar energy storage systems. *Renew. Sustain. Energy Rev.* **2010**, *14*, 1059–1069. [CrossRef]
5. Rosen, M.A. The exergy of stratified thermal energy storages. *Sol. Energy* **2001**, *71*, 173–185. [CrossRef]
6. Zanganeh, G.; Pedretti, A.; Haselbacher, A.; Steinfeld, A. Design of packed bed thermal energy storage systems for high-temperature industrial process heat. *Appl. Energy* **2015**, *137*, 812–822. [CrossRef]
7. Allen, K.G.; von Backström, T.W.; Kröger, D.G. Packed bed pressure drop dependence on particle shape, size distribution, packing arrangement and roughness. *Powder Technol.* **2013**, *246*, 590–600. [CrossRef]
8. Sarbu, I.; Sebarchievici, C. A comprehensive review of thermal energy storage. *Sustainability* **2018**, *10*, 191. [CrossRef]
9. Yang, B.; Wang, Y.; Bai, F.; Wang, Z. Experimental and numerical investigation of a packed-bed thermal energy storage device. *AIP Conf. Proc.* **2017**, *1850*. [CrossRef]
10. Yang, J.; Hu, Y.; Qian, P.; Guo, Z.; Wang, Q. Experimental Study of Forced Convective Heat Transfer in Packed Beds With Uniform and Non-Uniform Spheres. *Heat Transf. Eng.* **2020**, *41*, 351–360. [CrossRef]
11. Yang, J.; Wang, Q.; Zeng, M.; Nakayama, A. Computational study of forced convective heat transfer in structured packed beds with spherical or ellipsoidal particles. *Chem. Eng. Sci.* **2010**, *65*, 726–738. [CrossRef]
12. Agrawal, P.; Gautam, A.; Kunwar, A.; Kumar, M.; Chamoli, S. Performance assessment of heat transfer and friction characteristics of a packed bed heat storage system embedded with internal grooved cylinders. *Sol. Energy* **2018**, *161*, 148–158. [CrossRef]
13. Singh, H.; Saini, R.P.; Saini, J.S. Performance of a packed bed solar energy storage system having large sized elements with low void fraction. *Sol. Energy* **2013**, *87*, 22–34. [CrossRef]
14. Sagara, K.; Nakahara, N. Thermal performance and pressure drop of rock beds with large storage materials. *Sol. Energy* **1991**, *47*, 157–163. [CrossRef]
15. Domanski, R.; Fellah, G. Exergy as a tool for designing and operating thermal storage units. *J. Power Technol.* **1995**, 23–45.
16. Bellecci, C.; Conti, M. Thermal energy storage in a porous medium: An entropy generation approach in a power production perspective. *Nuovo Cim. C* **1992**, *15*, 275–287. [CrossRef]
17. Bejan, A. *Entropy Generation Minimization: The Method of Thermodynamic Optimization of Finite-Size Systems and Finite-Time Processes (Mechanical and Aerospace Engineering Series)*; CRC Press: Boca Raton, FL, USA, 1996; ISBN 0-8493-9651-4.
18. Osiecka, E. *Materiały Budowlane. Kamień—Ceramika—Szkło*; Oficyna Wydawnicza Politechniki Warszawskiej: Warsaw, Poland, 2010; ISBN 978-83-7207-865-0. (In Polish)
19. Nemś, M.; Nemś, A.; Pacyga, P. A Granite Bed Storage for a Small Solar Dryer. *Materials (Basel)* **2018**, *11*, 1969. [CrossRef]
20. Hartley, H.O. Smallest Composite Designs for Quadratic Response Surfaces. *Biometrics* **1959**. [CrossRef]
21. Singh, R.; Saini, R.P.; Saini, J.S. Nusselt number and friction factor correlations for packed bed solar energy storage system having large sized elements of different shapes. *Sol. Energy* **2006**, *80*, 760–771. [CrossRef]
22. Kostowski, E. *Zbiór Zadań z Przepływu Ciepła*; Wydawnictwo Politechniki Śląskiej: Gliwice, Poland, 2006; ISBN 83-88000-18-7. (In Polish)
23. Cengel, Y.A.; Boles, M.A. *Thermodynamics: An Engineering Approach*, 8th ed.; McGraw-Hill Education: New York, NY, USA, 2014; ISBN 9780073398174.
24. Ranz, W.E.; Marshall, W.R. Evaporation from drops. Parts I & II. *Chem. Eng. Progr.* **1952**. [CrossRef]
25. Melissari, B.; Argyropoulos, S.A. Development of a heat transfer dimensionless correlation for spheres immersed in a wide range of Prandtl number fluids. *Int. J. Heat Mass Transf.* **2005**, *48*, 4333–4341. [CrossRef]

26. Kunii, D.; Levenspiel, O. *Fluidization Engineering*, 2nd ed.; Elsevier: Cambridge, MA, USA, 1991; ISBN 0-409-90233-0.
27. Wiśniewski, S.; Wiśniewski, T.S. *Wymiana Ciepła*; Wydawnictwo WNT: Warsaw, Poland, 2013; ISBN 9788379260478. (In Polish)